Short Note

Multiscale Seismic Tomography and Earthquake Relocation Incorporating Differential Time Data: Application to the Maule Subduction Zone, Chile

by Jeremy D. Pesicek,[*] Haijiang Zhang, and Clifford H. Thurber

Abstract   We present a multiscale seismic tomography method incorporating differential time data. This is an extension of the double-difference tomography method to teleseismic distances using a nested regional–global model parameterization. It allows inclusion of absolute and differential time data observed at any distance, potentially improving resolution of structure in areas where local or regional data are sparse. The algorithm, named *teletomoDD*, is quite flexible and is applicable to a variety of relocation and tomography problems, including simultaneously solving for global velocity structure. To illustrate the technique, we apply it to the Maule region of Chile, where an M_w 8.8 earthquake occurred in 2010.

Introduction

Seismic arrival-time tomography has become a standard tool for seismologists investigating the structure and dynamics of various tectonic regions around the globe at a range of scales. For regional body-wave studies, there are two end-member techniques commonly in use: local earthquake tomography (LET; Aki and Lee, 1976; Thurber, 1983) and teleseismic tomography (Aki *et al.*, 1977). LET uses well-distributed sources and receivers located within the volume of interest, which ideally provide somewhat uniform body-wave sampling throughout the volume. In contrast, teleseismic tomography uses distant seismic sources to solve for the model region of interest beneath receivers, usually by assuming an *a priori* earth model outside the region. Both of these techniques have inherent advantages and pitfalls. For example, LET resolution suffers when the source distribution (and hence ray coverage) is nonuniform. In contrast, teleseismic tomography studies generally have more uniform ray coverage, but do not fully account for aspherical structure and source location uncertainty outside the model volume. For more thorough reviews, the reader is referred to Thurber and Aki (1987), Rawlinson and Sambridge (2003), Thurber (2003), Thurber and Ritsema (2007), and Rawlinson *et al.* (2010). Because of these fundamental differences in methodology and applicability, tomographers have sought to bridge the gap between these two tomography techniques, attempting to combine advantages of each while mitigating their inherent limitations. Such efforts seek to improve tomographic imaging by incorporating all possible data from body waves passing through a particular region, regardless of the locations of sources and receivers. These multiscale methods have been developed and employed in a variety of ways by various authors (e.g., Zhao *et al.*, 1994; Widiyantoro and van der Hilst, 1996; Bijwaard *et al.*, 1998; Zhao, 2009).

In addition to multiscale techniques, another recent development in tomographic methodology comes from the use of relative arrival times for pairs of events. These differential (or double difference [DD]) data have been used to improve earthquake locations using data observed at local (Waldhauser and Ellsworth, 2000) to teleseismic distances (Waldhauser and Schaff, 2007; Pesicek, Thurber, Zhang, *et al.*, 2010). In tomographic studies, the use of such data has been shown to improve imaging in many local and regional studies (Zhang and Thurber, 2006). As is true in location studies, the use of differential data in tomography is not limited to local or regional distances; here we report on the extension of their use to teleseismic distances. Our multiscale tomography technique, including differential data, can be applied in any environment but is especially useful when local data are sparse, such as in poorly instrumented subduction zones. Even when local/regional data are dense, incorporating teleseismic events can provide resolution beyond the reaches of regional data, such as beneath slab seismicity and outboard of the coast. Furthermore, in contrast to the conventional teleseismic tomography method that focuses specifically on imaging the model region beneath the receiver array, our new method is also applicable to solving for structure near earthquakes using teleseismic data.

*Now at Spectraseis Inc., 1899 Wynkoop Street, Suite 350, Denver, Colorado 80202.

We recently applied a teleseismic DD location technique to improve earthquake hypocenters in the Sumatra region (Pesicek, Thurber, Zhang, *et al.*, 2010). In this paper, we utilize DD data for the determination of a regional velocity model as well, including simultaneously solving for global velocity structure. We present an example application using data from the Maule region of south central Chile, South America, where an M_w 8.8 earthquake occurred in 2010.

Method

Similar to the local scale DD tomography method (Zhang and Thurber, 2003), we can represent its extension to teleseismic distance using the following equations:

$$r_k^i = \sum_{l=1}^{3} \frac{\partial T_k^i}{\partial x_l^i} \Delta x_l^i + \Delta \tau^i + \sum_{n \in G} w_n^G \delta u_n^G + \sum_{n \in L} w_n^L \delta u_n^L + s_k \tag{1}$$

for absolute data, and

$$\begin{aligned}
dr_k^{ij} &= r_k^i - r_k^j \\
&= \sum_{l=1}^{3} \frac{\partial T_k^i}{\partial x_l^i} \Delta x_l^i + \Delta \tau^i + \sum_{n \in L}^{ik} w_n^L \delta u_n^L \\
&\quad - \left(\sum_{l=1}^{3} \frac{\partial T_k^j}{\partial x_l^j} \Delta x_l^j + \Delta \tau^j + \sum_{n \in L}^{jk} w_n^L \delta u_n^L \right)
\end{aligned} \tag{2}$$

for differential data. In the above equations, r_k^i and r_k^j are the arrival-time residuals for events i and j at station k, dr_k^{ij} is the residual (double) difference, $\Delta \tau^i$ is the origin time perturbation for event i, $\Delta x_l^i (l = 1, 2, 3)$ are the location perturbations in the three coordinate directions, δu_n^G and δu_n^L are slowness perturbations for global (G) and local (L) models, respectively, w_n^G and w_n^L are the weighted ray lengths with respect to global and local model nodes (n), and s_k is the station correction. A global and regional model are used, but global velocity nodes inside the regional model are assigned their values by interpolation among the surrounding regional nodes and are not included in the inversion. The global model is resolved only using the absolute times; the differential times for teleseismic stations are only sensitive to the regional model because the teleseismic ray paths effectively coincide outside the regional model.

Our algorithm that realizes the above multiscale tomography method, including differential data, is named *teletomoDD*. It is a global extension of the DD LET algorithm *tomoDD* (Zhang and Thurber, 2003), which in turn is based on the DD relocation algorithm *hypoDD* (Waldhauser and Ellsworth, 2000) and the LET algorithm *simul* (Thurber, 1983, 1984; Evans *et al.*, 1994; Thurber and Eberhart-Phillips, 1999), all of which are publicly available and widely used. Our goal with *teletomoDD* is to improve tomographic imaging and event locations in a specific region of interest by including all possible body-wave arrival and dif-

ferential time data observed at any distance. In order to properly constrain velocity anomalies along portions of seismic rays outside the regional model, we require a spherical Earth travel-time predictor, a global reference velocity model, and the capability to determine whole Earth velocity structure. To accomplish this, we have taken an approach similar to the nested regional–global method developed by Widiyantoro and van der Hilst (1996, 1997), adapted and modified by us for use in the Sumatra (Pesicek *et al.*, 2008; Pesicek, Thurber, Widiyantoro, *et al.*, 2010) and Maule (Pesicek *et al.*, 2012) regions. In this method, a finely gridded regional model is built around the volume of interest, which is then surrounded by a coarser global model (Fig. 1). However, in contrast to the regular grid spacing and constant slowness cells inherent in this technique, *teletomoDD* retains the non-uniform node parameterization capability (with interpolation between nodes) built into *simul* and *tomoDD*, allowing more flexibility when designing the parameterization. To determine ray paths and calculate travel times in a spherical Earth, we have utilized the pseudobending (PB) method of Um and Thurber (1987) as extended to spherical coordinates by Koketsu and Sekine (1998). In addition to tracing rays for primary P phases, we have modified the PB ray tracer to also trace rays for the depth phases pP and pwP, which are helpful for increasing shallow ray sampling and better constraining focal depth. We trace depth phases to initial bounce point estimates, which are then iteratively perturbed until the angles between the upgoing and downgoing ray segments are equal (Zhao and Lei, 2004).

Sensitivity Matrix Construction and Inversion

When including differential data, only slowness derivatives near the sources are included. For teleseismic data especially, including differential derivatives along the entire length of the two ray paths is unnecessary and potentially numerically troublesome because they tend to rapidly approach zero outside the source regions. We include slowness derivatives to a distance "facray" times the event pair offset and have chosen facray = 1.5, following Eberhart-Phillips and Reyners (2012).

We apply the conjugate gradient solver *LSQR* (Paige and Saunders, 1982) to obtain our solution. This approximate technique is widely used due to its computational efficiency when determining large numbers of parameters. Accuracy of the *LSQR* solution depends on the scaling of the problem. LET studies employing *LSQR* often scale the derivatives by the Euclidean length column. This type of scaling tends to distribute model perturbations evenly across all parameters. Although this scaling is sufficient in many cases, it can also be problematic when different types of parameters are included and in cases where ray sampling is highly uneven. As an alternative, we have implemented volume scaling (Nolet, 1987; Spakman and Nolet, 1988) as an option in *teletomoDD*. The design of our nested regional–global model is such that velocities at nodes in the global model typically
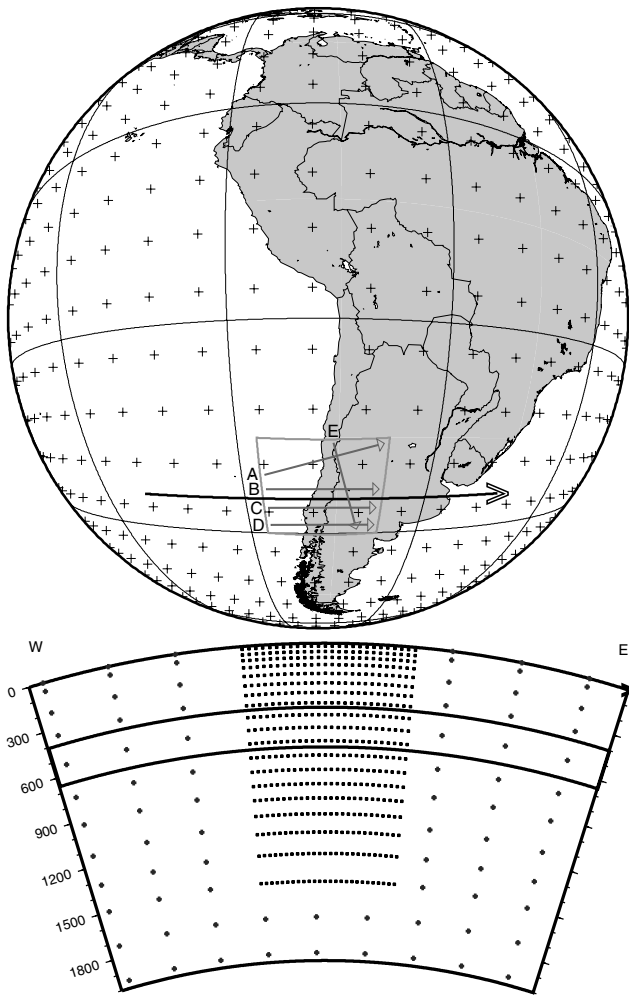
In addition to scaling, we also regularize the problem with minimum norm damping and first-difference smoothing. Damping and smoothing are applied independently to the global and regional velocity terms; location terms are also independently damped. Together with the volume scaling, properly testing and tuning the regularization coefficients allows the user the flexibility to properly balance the distribution of perturbations across all parameters. Although this flexibility is built into *teletomoDD*, our experience has shown that the volume scaling automates this perturbation balancing and reduces the subjectivity of choosing the relative values of the various regularization coefficients for the model. In this way, the scaling of the sensitivity matrix automatically distributes the perturbations based on the node spacing, which is based directly on the model design and data distribution. Small relative differences in the regularization coefficients have little effect on the solution. The values should be chosen based on the overall level of data noise and expected level of perturbation to the reference model.

Data Selection and Weighting Strategies

A variety of different data types can be used in *teletomoDD* for relocation and tomography purposes. Although we seek to improve event locations and tomographic imaging by the use of DD data, such data alone are insufficient for most applications. As in the local case (*tomoDD*), *teletomoDD* also allows the inclusion of absolute arrival-time data, in order to improve both absolute location accuracy and velocity resolution outside the source regions. All data are weighted by pick quality, and differential data are further weighted by event separation distance (Waldhauser and Ellsworth, 2000) and by the angle between the ray takeoff direction and the vector connecting the two events (Waldhauser and Schaff, 2007). Finally, any event can be treated as a shot, allowing the user to fix origin times and/or hypocentral parameters for particular events if desired.

The strategy for the formation and incorporation of differential data may differ depending on the specific goals of a particular study, and ideal parameters for the relocation-only problem are likely not ideal for the joint location and tomography problem. For relocation purposes, DD data for very closely spaced events are likely to improve their relative locations. However, for tomography, events that are very closely spaced (much closer than the node separation) provide limited additional velocity constraints. In addition, small DD slowness derivatives outside the source region may negatively impact the solution. In contrast, event pairs that are too far apart have less similar ray paths that are more likely to sample distinct velocity anomalies. Because absolute arrival times for events are usually also included in the inversion, DD data for event pairs with large separation distances do not necessarily provide new constraints. For these reasons, the selection of differential data is an important task requiring careful consideration.

Figure 1. Nested regional–global model design. In this example for the Maule region of Chile (box), the global model has uniform 5° lateral node separation and the regional model has 0.5° node separation, following Pesicek *et al.* (2012). Node separation is not required to be uniform in *teletomoDD*. Locations of cross sections A–E for Figures 3 and 5 are also shown and are the same as those in Pesicek *et al.* (2012).

represent volumes of the Earth much larger than those in the regional model. In addition, within both the regional and global models, node spacing will generally increase with depth, reflecting the reduction of ray sampling with depth. Such variable node spacing can have the effect of attributing larger slowness anomalies to areas with larger node spacing (Nolet, 1987; Spakman and Nolet, 1988). To counteract this effect, we prefer to scale the slowness derivatives by the volume that each node represents. With this strategy, we scale the location derivatives by the mean node volume, but we have found that the specific scaling of the location derivatives is unimportant because the location perturbations remain unresolved in the joint solution using *LSQR* no matter how they are scaled (Pesicek, Thurber, Widiyantoro, *et al.*, 2010). Thus, we relocate the events in a subsequent step using the updated model, as discussed in the Application to the Maule Region section.

To form the catalog differential times for the purpose of relocation, we link each event with its 20 nearest neighbors within 300 km that have at least 15 commonly observed phases at stations within 90° (Waldhauser and Schaff, 2007; Pesicek, Thurber, Zhang, *et al.*, 2010). Owing to the importance of the depth phase data for constraining focal depth despite their relative paucity, we relax these conditions to form depth phase differential times and required only two links per neighbor and two links per pair. For tomography purposes, we define a minimum event separation of 3 km and require that the distance to the station be four times greater than the event pair separation. We further filter the data by azimuth and distance to reduce observation bias and provide more uniformly distributed differential data. Similar filtering of the global and regional absolute data is also performed (e.g. Widiyantoro and van der Hilst, 1997).

To properly account for the varying data quantities, types, and qualities, we apply a hierarchical dynamic weighting scheme to the data (Waldhauser and Ellsworth, 2000; Zhang and Thurber, 2003). We initially give the absolute data high weighting, because they control the absolute locations and large-scale structures. We then progressively lower their weighting during subsequent iterations. Conversely, we progressively increase the weighting of the differential times during iterations. If available, cross-correlation data are weighted the highest in final iterations to allow these more precise data to control the final locations and model changes.

Application to the Maule Region

In the Maule region, we start with the absolute dataset used by Pesicek *et al.* (2012) to form differential times. These data consist of reprocessed teleseismic data for 2605 cataloged earthquakes in the Maule region reported by the International Seismological Centre and National Earthquake Information Center (NEIC) for the 11 February 1960–9 September 2010 time period using the Engdahl, van der Hilst, and Buland (EHB) single event relocation method (Engdahl *et al.*, 1998). To improve event location accuracy, we obtained and included additional phases in the relocation procedure recorded by the International Maule Aftershock Dataset (IMAD) network (Lange *et al.* 2012; Rietbrock *et al.*, 2012; Hayes *et al.*, 2013). For aftershocks, we included 4977 *P* phases from 267 larger events. To increase focal depth constraint, we also included 3839 reported depth phases (*pP*, *sP*, and *pwP*) that until recently were not used routinely by global location agencies. The combined catalog of phase data was then reprocessed using the EHB method, and the *P* data were further processed to form differential data for tomography as described in the Data Selection and Weighting Strategies section.

Iteratively solving the joint location and tomography problem for the whole Earth, including global data and regional differential data, is feasible but remains computationally burdensome. Furthermore, it does not allow for easy analysis of the effects of the various data types and particular parameters, which may need to change for each iteration. In
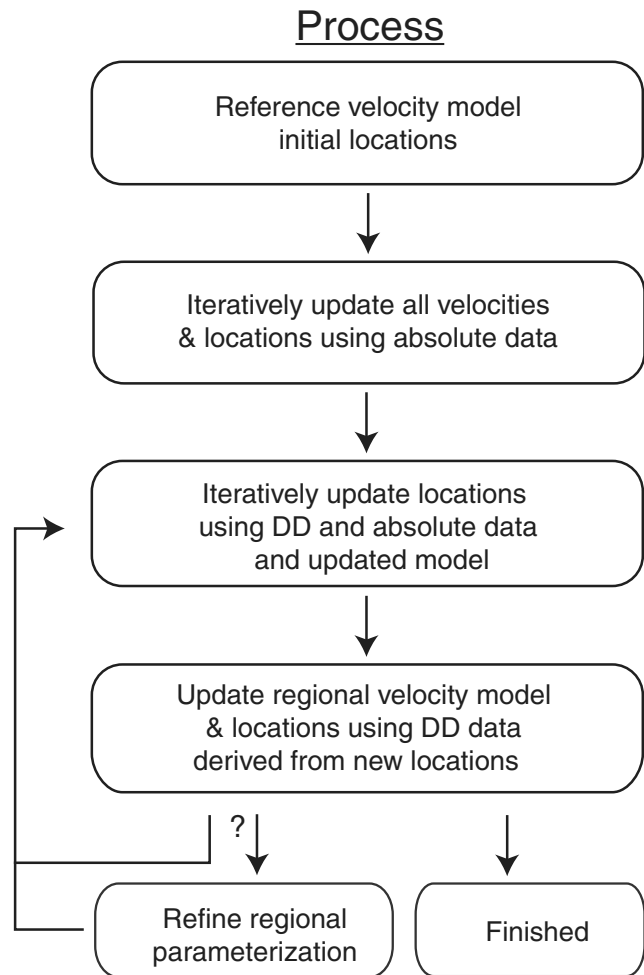
Process

Figure 2. Organizational flowchart showing inversion sequence for application of *teletomoDD*.

many cases it may be more desirable to proceed in a more sequential fashion, carefully assessing the input data and results at each step while progressing toward a final event location catalog and model. In the Maule region, we used a sequential approach shown in Figure 2 and described as follows. In the first step, we selected a set of regional and global arrival-time data to include in a joint inversion for regional and global structure. In this step, we started with a 3D reference model for both the global (Li *et al.*, 2008) and regional (Pesicek *et al.*, 2012) model volumes. These reference models were produced using linear, single iteration techniques commonly used in global tomography studies. However, many studies have shown the improvements possible by performing multiple iterations of the linearized inversion using 3D ray tracing at each step (Bijwaard and Spakman, 2000; Widiyantoro *et al.*, 2000; Gorbatov *et al.*, 2001; Pesicek, Thurber, Widiyantoro, *et al.*, 2010), as is routinely done in LET studies. To improve imaging of the mantle structure in the regional model, we first performed several iterations using a combined global and regional data set and the same parameterization as used by Pesicek *et al.* (2012). The results
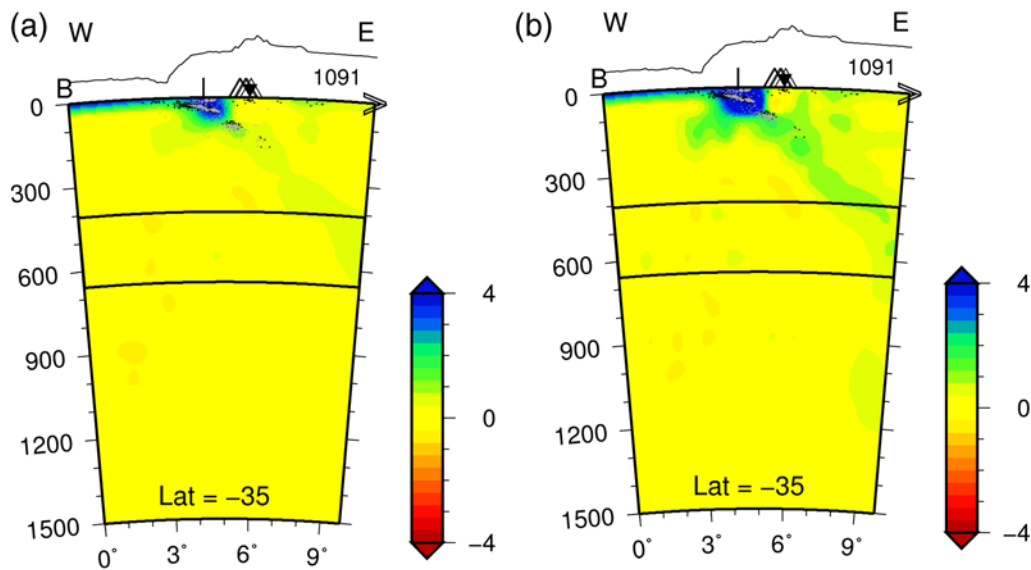
Figure 3. (a) Single iteration results from Pesicek *et al.* (2012). (b) Iterative solution obtained using *teletomoDD* without DD data, as described in text. The scale shows percent perturbation relative to the reference model. Triangles at the surface show volcano locations, and the vertical line and inverted triangle show the locations of the coastline and international border, respectively. The cross-section location is shown in Figure 1, and its length in km is shown at the top right of the section. Exaggerated topography (20×) is also shown. The color version of this figure is available only in the electronic edition.

show that the velocity anomaly patterns from multiple iterations are quite similar in pattern to the single iteration but with increased amplitudes in the slab and other features (Fig. 3), with an average absolute perturbation to the regional model of 0.52% and a maximum perturbation of 10%.

The second step in our sequential approach is to relocate events in the region using the updated velocity model. For this step, we use absolute arrival-time data and differential data and solve only for location and origin time perturbations. Although location derivatives are included in every inversion step, the location changes resulting from the joint inversions alone are generally inadequate for obtaining convergent locations, as is the case for LET due to the more nonlinear nature of the earthquake location problem. Thus, we prefer to separately determine the locations in the updated velocity model iteratively, following Pesicek, Thurber, Zhang, *et al.* (2010). In the Maule region, we take advantage of the dense aftershock data recorded by the IMAD deployment (Lange *et al.*, 2012). Many large aftershocks observed locally by IMAD were also recorded teleseismically (267 events; Pesicek *et al.*, 2012), thus providing us the opportunity to link events across scales and time periods through the use of DD data at common stations. To further improve the teleseismic locations, we have jointly relocated the teleseismic catalog with well-constrained IMAD events from the Lange *et al.* (2012) catalog (Fig. 4).

The DD relocations (Fig. 4c) agree well with the local IMAD locations (Fig. 4d) and are able to define the location of the slab better than the NEIC (Fig. 4a) and EHB (Fig. 4b) locations. The DD data links events with poorly constrained depths to other better constrained events, allowing us to obtain free depth solutions for all the EHB starting locations, many of which were fixed in depth by the EHB method. The

combined use of differential and absolute arrival-time data and a high-resolution 3D velocity model allows us to obtain well constrained absolute and relative locations for teleseismically recorded events, with lower uncertainties compared to the EHB method (Pesicek, Thurber, Zhang, *et al.*, 2010).

We can make a quantitative comparison of these various location estimates to gauge the success of the *teletomoDD* results. We adopt the Lange *et al.* (2012) IMAD locations as the reference locations, presuming them to be most accurate, and assess the differences between the three other location estimates and IMAD. Table 1 presents the results of that comparison. Note that the number of events in common varies among the different sets of locations. As could be expected, the NEIC locations show the greatest deviations from IMAD, with standard deviations of ∼10 km or more in all directions, and also a large mean shift in depth. The EHB standard deviations are about half the size of those for NEIC, and the *teletomoDD* standard deviations are smaller still. Thus, the quality of the *teletomoDD* locations approaches that of the IMAD locations obtained using a local network.

The third step is to improve the tomographic model using the new event locations and differential data (Fig. 5). In this step, a new set of differential data is constructed, distinct from the differential data used for relocation in the previous step, as the event locations have changed. These DD data are more carefully groomed for tomography purposes as discussed in the Data Selection and Weighting Strategies section. In this step, the regional model parameterization could be redefined with a closer node spacing (Fig. 2) to allow the differential data to resolve finer scale structures in the source regions. However, in this paper, we retain the same parameterization throughout in order to better illustrate the changes due
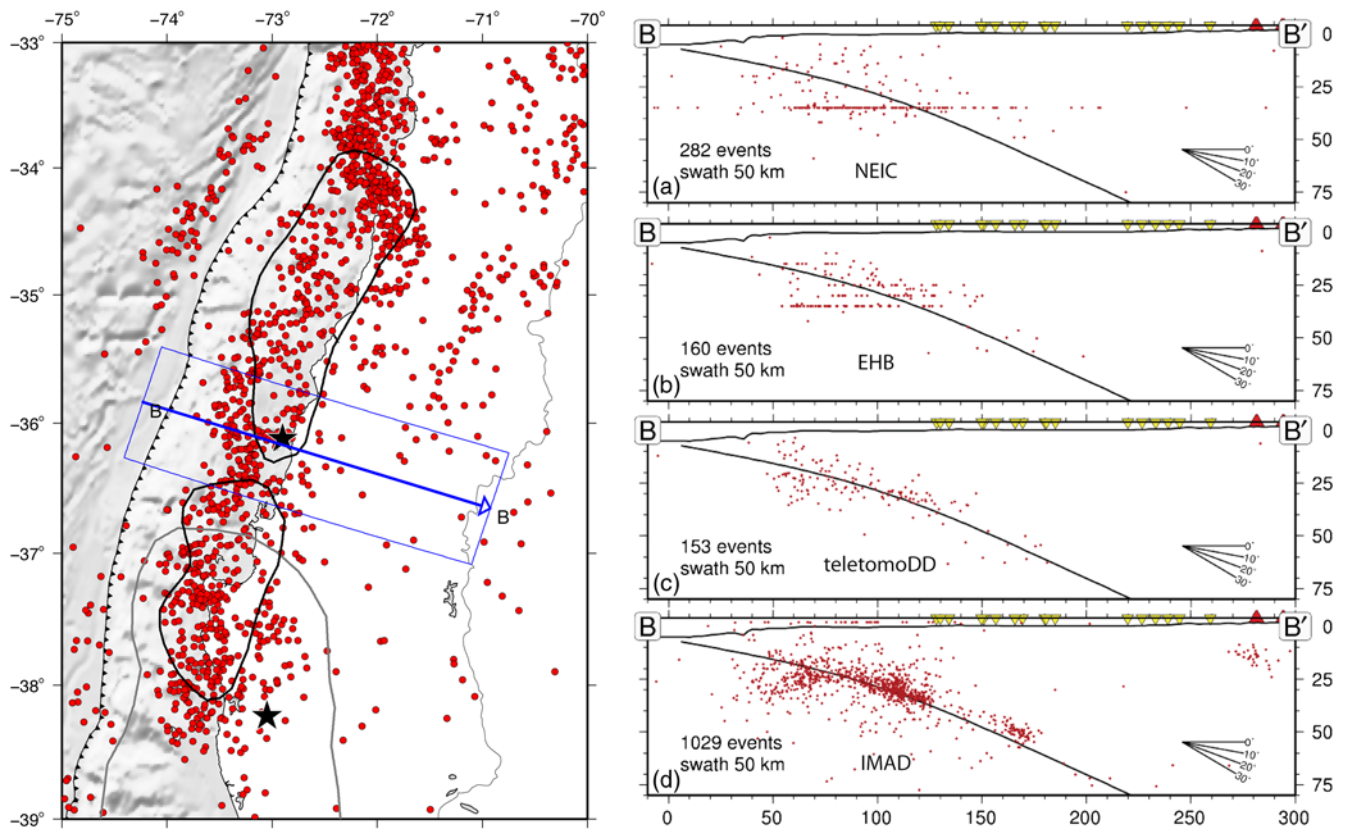
Figure 4. Comparison of event depths on a cross section taken perpendicular to the trench along the B–B′ line of Lange *et al.* (2012). The cross section lies north of the 1960 M_w 9.5 mainshock epicenter (star; rupture area in gray) and just south of the 2010 Maule mainshock epicenter (star; rupture areas in black). (a) NEIC and (d) IMAD profiles modified from Lange *et al.* (2012). IMAD stations (inverted triangles), volcanoes (triangles), and estimated interface (black line; Hayes *et al.*, 2009) are shown. Panel (b) shows EHB locations, which serve as the initial locations for solutions shown in (c). All events shown in (b) have been relocated successfully. The difference in numbers of events in (b) versus (c) is due to the EHB locations moving laterally outside of the cross section. The color version of this figure is available only in the electronic edition.

to the incorporation of differential data. Because we are only using differential data from regional sources with slowness derivatives confined to the near source areas, we do not solve for global structure in this inversion step.

For this step, the average absolute perturbation to the regional model is 0.09% with a maximum perturbation of 5%. Figure 5 shows that the changes to the velocity model due to the teleseismic differential times mainly occur in the vicinity of the slab seismicity, as expected. Larger changes occur at shallower depths where the seismicity is densest (e.g., Fig. 5a,c, 0–100 km depth), and few if any changes occur where seismicity is sparse (Fig. 5d). The changes beneath slab seismicity are predominantly positive increases in *P*-wave velocity while changes above the slab in the mantle wedge

are primarily negative (e.g., Fig. 5b). These results are consistent with the fact that teleseismic tomography methods used to generate the reference model tend to underestimate the amplitudes of mantle velocity structures (e.g. Thurber and Ritsema, 2007). At the current scale, the addition of DD data serves primarily to obtain more accurate slab and other anomaly amplitudes in the source regions. However, resolution of smaller structures, such as intraslab anomalies, may be possible with further grid refinement.

Conclusions

The multiscale tomography and relocation method we present provides several advantages over other common

Table 1
Deviations of the NEIC, EHB, and *teletomoDD* Locations from the Lange *et al.* (2012) IMAD Locations

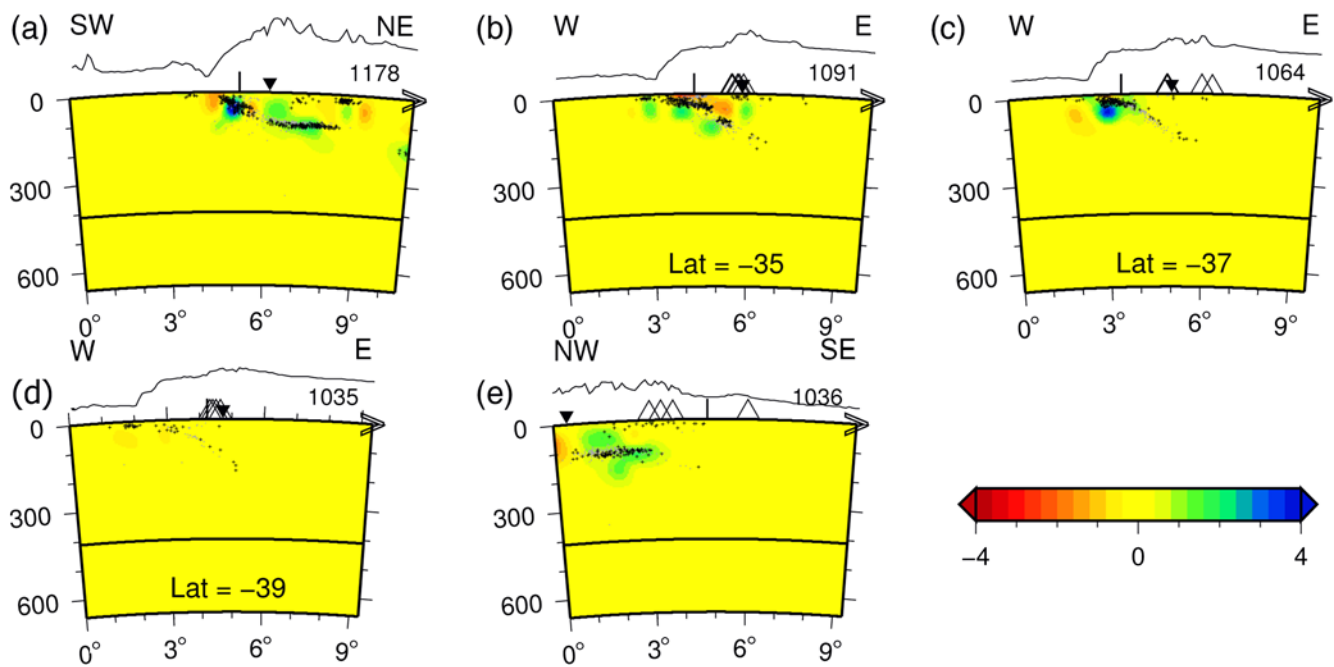|	NEIC (456 Events) Latitude (°); Longitude (°); Depth (km)	EHB (1909 Events) Latitude (°); Longitude (°); Depth (km)	*teletomoDD* (1602 Events) Latitude (°); Longitude (°); Depth (km)
σ	0.087; 0.167; 14.44	0.038; 0.064; 6.38	0.019; 0.053; 4.18
Mean	−0.021; −0.071; 6.51	−0.002; 0.011; −0.73	−0.001; 0.013; −0.64

Figure 5. Perturbations to intermediate reference model (shown in Fig. 3b) using only regional DD data. Cross-section locations are shown in Figure 1. Other features are as in Figure 3. The color version of this figure is available only in the electronic edition.

tomography techniques that might be used for similar regional problems. In comparison to other teleseismic tomography algorithms, *teletomoDD* is able to properly treat absolute and differential data for phases at any distance. By iterating the regional–global inversion process, we obtain an improved model for subsequent relocation analysis. Furthermore, by including differential data, we are able to improve source locations and velocity resolution near the sources. In comparison to local/regional techniques, we are able to improve resolution beyond the reach of the local/regional data, such as beneath the sources. In addition, the inclusion of teleseismic phases provides additional constraints on hypocentral parameters that might be biased by limited local observations. When applied to the Maule region, the method improves mantle slab imaging, location accuracy, and resolution near the sources.

Data and Resources

All data used in this paper came from published sources listed in the references. Most of the plots were made using the Generic Mapping Tools version 4.5.5 (www.soest.hawaii.edu/gmt; Wessel and Smith, 1998; last accessed March 2013)

Acknowledgments

References

Aki, K., and W. H. K. Lee (1976). Determination of three-dimensional velocity anomalies under a seismic array using first *P* arrival times from local earthquakes: 1. A homogeneous initial model, *J. Geophys. Res.* **81,** no. 23, 4381–4399, doi: 10.1029/JB081i023p04381.

Aki, K., A. Christoffersson, and E. S. Husebye (1977). Determination of the three-dimensional seismic structure of the lithosphere, *J. Geophys. Res.* **82,** no. 2, 277–296, doi: 10.1029/JB082i002p00277.

Bijwaard, H., and W. Spakman (2000). Non-linear global *P*-wave tomography by iterated linearized inversion, *Geophys. J. Int.* **141,** 71–82, doi: 10.1046/j.1365-246X.2000.00053.x.

Bijwaard, H., W. Spakman, and E. R. Engdahl (1998). Closing the gap between regional and global travel time tomography, *J. Geophys. Res.* **103,** no. B12, 30,055–30,078, doi: 10.1029/98JB02467.

Eberhart-Phillips, D., and M. Reyners (2012). Imaging the Hikurangi plate interface region, with improved local-earthquake tomography, *Geophys. J. Int.* **190,** no. 2, 1221–1242, doi: 10.1111/j.1365-246X.2012.05553.x.

Engdahl, E. R., R. van der Hilst, and R. Buland (1998). Global teleseismic earthquake relocation with improved travel times and procedures for depth determination, *Bull. Seismol. Soc. Am.* **88,** 722–743.

Evans, J. R., D. Eberhart-Phillips, and C. H. Thurber (1994). User's manual for SIMULPS12 for imaging V_P and V_P/V_S: A derivative of the Thurber tomographic inversion SIMUL3 for local earthquakes and explosions, *U.S. Geol. Surv. Open-File Rept. OFR 94-431*, 101 pp.

Gorbatov, A., Y. Fukao, and S. Widiyantoro (2001). Application of a three-dimensional ray-tracing technique to global *P*, *PP* and *Pdiff* traveltime tomography, *Geophys. J. Int.* **146,** no. 3, 583–593, doi: 10.1046/j.0956-540x.2001.01487.x.

Hayes, G. P., E. Bergman, K. L. Johnson, H. M. Benz, L. Brown, and A. S. Meltzer (2013). Seismotectonic framework of the 2010 February 27 M_w 8.8 Maule, Chile earthquake sequence, *Geophys. J. Int.* **195,** no. 2, 1034–1051, doi: 10.1093/gji/ggt238.

Hayes, G. P., D. J. Wald, and K. Keranen (2009). Advancing techniques to constrain the geometry of the seismic rupture plane on subduction interfaces *a priori*: Higher-order functional fits, *Geochem. Geophys. Geosyst.* **10,** no. 9, doi: 10.1029/2009GC002633.

Koketsu, K., and S. Sekine (1998). Pseudo-bending method for three-dimensional seismic ray tracing in a spherical earth with discontinuities, *Geophys. J. Int.* **132,** no. 2, 339–346, doi: 10.1046/j.1365-246x.1998.00427.x.

Lange, D., F. Tilmann, S. E. Barrientos, E. Contreras-Reyes, P. Methe, M. Moreno, B. Heit, H. Agurto, P. Bernard, J.-P. Vilotte, and S. Beck (2012). Aftershock seismicity of the 27 February 2010 M_w 8.8 Maule earthquake rupture zone, *Earth Planet. Sci. Lett.* **317–318,** 413–425.

Li, C., R. D. van der Hilst, E. R. Engdahl, and S. Burdick (2008). A new global model for *P* wave speed variations in Earth's mantle, *Geochem. Geophys. Geosyst.* **9,** no. 5, doi: 10.1029/2007GC001806.

Nolet, G. (1987). *Seismic Wave Propagation and Seismic Tomography; with Applications in Global Seismology and Exploration Geophysics*, D. Reidel Publ. Co., Dordrecht, The Netherlands.

Paige, C. C., and M. A. Saunders (1982). LSQR: An algorithm for sparse linear equations and sparse least squares, *ACM Trans. Math. Software* **8,** no. 1, 43–71, doi: 10.1145/355984.355989.

Pesicek, J. D., E. R. Engdahl, C. H. Thurber, H. R. DeShon, and D. Lange (2012). Mantle subducting slab structure in the region of the 2010 *M* 8.8 Maule earthquake (30–40° S), Chile, *Geophys. J. Int.* doi: 10.1111/j.1365-246X.2012.05624.x.

Pesicek, J. D., C. H. Thurber, S. Widiyantoro, E. R. Engdahl, and H. R. DeShon (2008). Complex slab subduction beneath northern Sumatra, *Geophys. Res. Lett.* **35,** no. 20, doi: 10.1029/2008GL035262.

Pesicek, J. D., C. H. Thurber, S. Widiyantoro, H. Zhang, H. R. DeShon, and E. R. Engdahl (2010). Sharpening the tomographic image of the subducting slab below Sumatra, the Andaman Islands and Burma, *Geophys. J. Int.* **182,** no. 1, 433–453, doi: 10.1111/j.1365-246X.2010.04630.x.

Pesicek, J. D., C. H. Thurber, H. Zhang, H. R. DeShon, E. R. Engdahl, and S. Widiyantoro (2010). Teleseismic double-difference relocation of earthquakes along the Sumatra-Andaman subduction zone using a 3-D model, *J. Geophys. Res.* **115,** no. B10, doi: 10.1029/2010JB007443.

Rawlinson, N., and M. Sambridge (2003). Seismic traveltime tomography of the crust and lithosphere, in *Advances in Geophysics*, Vol. 46, Elsevier, Amsterdam, 81–198.

Rawlinson, N., S. Pozgay, and S. Fishwick (2010). Seismic tomography: A window into deep Earth, *Phys. Earth Planet. In.* **178,** no. 3–4, 101–135, doi: 10.1016/j.pepi.2009.10.002.

Rietbrock, A., I. Ryder, G. Hayes, C. Haberland, D. Comte, S. Roecker, and H. Lyon-Caen (2012). Aftershock seismicity of the 2010 Maule $M_w = 8.8$, Chile, earthquake: Correlation between co-seismic slip models and aftershock distribution? *Geophys. Res. Lett.* **39,** no. 8, L08310, doi: 10.1029/2012GL051308.

Spakman, W., and G. Nolet (1988). Imaging algorithms, accuracy and resolution in delay time tomography, in *Mathematical Geophysics: A Survey of Recent Developments in Seismology and Geodynamics*, N. J. Vlaar, G. Nolet, M. J. R. Wortel, and S. A. P. L. Cloetingh (Editors), D. Reidel Publ. Co., Dordrecht, The Netherlands (NLD), 155–188.

Thurber, C. H. (1983). Earthquake locations and three-dimensional crustal structure in the Coyote Lake Area, central California, *J. Geophys. Res.* **88,** no. B10, 8226–8236, doi: 10.1029/JB088iB10p08226.

Thurber, C. H. (1984). SIMUL3, in *Documentation of Earthquake Algorithms*, E. R. Engdahl (Editor), World Data Center A for Solid Earth Geophysics, Washington, D.C., 15–17.

Thurber, C. H. (2003). Seismic tomography of the lithosphere with body waves, *Pure Appl. Geophys.* **160,** no. 3–4, 717–737, doi: 10.1007/PL00012555.

Thurber, C. H., and K. Aki (1987). Three-dimensional seismic imaging, *Annu. Rev. Earth Planet. Sci.* **15,** no. 1, 115–139, doi: 10.1146/annurev.ea.15.050187.000555.

Thurber, C., and D. Eberhart-Phillips (1999). Local earthquake tomography with flexible gridding, *Comput. Geosci.* **25,** no. 7, 809–818, doi: 10.1016/S0098-3004(99)00007-2.

Thurber, C., and J. Ritsema (2007). Theory and observations—Seismic tomography and inverse methods, *Treatise on Geophysics* **1,** 323–360.

Um, J., and C. Thurber (1987). A fast algorithm for two-point seismic ray tracing, *Bull. Seismol. Soc. Am.* **77,** no. 3, 972–986.

Waldhauser, F., and W. L. Ellsworth (2000). A double-difference earthquake location algorithm: Method and application to the Northern Hayward fault, California, *Bull. Seismol. Soc. Am.* **90,** no. 6, 1353–1368, doi: 10.1785/0120000006.

Waldhauser, F., and D. Schaff (2007). Regional and teleseismic double-difference earthquake relocation using waveform cross-correlation and global bulletin data, *J. Geophys. Res.* **112,** no. B12, doi: 10.1029/2007JB004938.

Wessel, P., and W. H. F. Smith (1998). New, improved version of the Generic Mapping Tools Released, *Eos Trans. AGU* **79,** 579.

Widiyantoro, S., and R. van der Hilst (1996). Structure and evolution of lithospheric slab beneath the Sunda Arc, Indonesia, *Science* **271,** no. 5255, 1566–1570, doi: 10.1126/science.271.5255.1566.

Widiyantoro, S., and R. van der Hilst (1997). Mantle structure beneath Indonesia inferred from high-resolution tomographic imaging, *Geophys. J. Int.* **130,** no. 1, 167–182, doi: 10.1111/j.1365-246X.1997.tb00996.x.

Widiyantoro, S., A. Gorbatov, B. L. N. Kennett, and Y. Fukao (2000). Improving global shear wave traveltime tomography using three-dimensional ray tracing and iterative inversion, *Geophys. J. Int.* **141,** no. 3, 747–758, doi: 10.1046/j.1365-246x.2000.00112.x.

Zhang, H., and C. H. Thurber (2003). Double-difference tomography: The method and its application to the Hayward fault, California, *Bull. Seismol. Soc. Am.* **93,** no. 5, 1875–1889, doi: 10.1785/0120020190.

Zhang, H., and C. Thurber (2006). Development and applications of double-difference seismic tomography, *Pure Appl. Geophys.* **163,** nos. 2–3, 373–403, doi: 10.1007/s00024-005-0021-y.

Zhao, D. (2009). Multiscale seismic tomography and mantle dynamics, *Gondwana Res.* **15,** no. 3–4, 297–323, doi: 10.1016/j.gr.2008.07.003.

Zhao, D., and J. Lei (2004). Seismic ray path variations in a 3D global velocity model, *Phys. Earth Planet. In.* **141,** no. 3, 153–166, doi: 10.1016/j.pepi.2003.11.010.

Zhao, D., A. Hasegawa, and H. Kanamori (1994). Deep structure of Japan subduction zone as derived from local, regional, and teleseismic events, *J. Geophys. Res.* **99,** no. B11, 22,313–22,329, doi: 10.1029/94JB01149.

University of Wisconsin–Madison
Department of Geoscience
1215 W Dayton Street
Madison, Wisconsin 53706
(J.D.P., C.H.T.)

Laboratory of Seismology and Physics of Earth's Interior
University of Science and Technology of China
96 Jinzhai Road, Hefei
Anhui 230026, China
(H.Z.)